Bright Trion Emission from Semiconductor Nanoplatelets

Lintao Peng[†], *Matthew Otten*[†], *Igor Coropceanu*[‡], *Moritz Cygorek*[‖], *Gary P. Wiederrecht*[†], *Pawel Hawrylak*[‖], *Dmitri Talapin*[‡], *Xuedan Ma*[*†]

[†]Center for Nanoscale Materials, Argonne National Laboratory, Lemont, Illinois 60439, United States

[‡]Department of Chemistry and James Franck Institute, University of Chicago, Chicago, Illinois 60637, United States

[‖]Department of Physics, University of Ottawa, Ottawa, Ontario, Canada K1N 6N5

Trion, a quasiparticle comprising one exciton and an additional charge carrier[1], offers unique opportunities for generating spin-photon entanglement[2, 3] that can be used in quantum switches[4], quantum repeaters[5], and quantum teleportation[6], all highly relevant for developing quantum networks. However, formation of trions in strongly confined low-dimensional materials is often deemed detrimental[7]. This is because trion emission in such materials is typically prohibited due to the predominant nonradiative Auger recombination processes[8]. Semiconductor nanoplatelets with their strong confinement in the thickness direction and extended lateral geometries exhibit large exciton coherence sizes[9] and reduced carrier-carrier interactions[10] that may enable unprecedented trion properties. Here we perform optical spectroscopic studies of individual CdSe nanoplatelets at cryogenic temperatures and observe bright trion emission with intensities comparable to that of

neutral exciton emission. Our theoretical modeling reveals distinct size-tunable trion states in the nanoplatelets that is advantageous for efficient trion emission. These properties make semiconductor nanoplatelets potential candidates as photon sources for spin-photon interface based quantum devices[4, 5, 11].

Strongly confined low-dimensional materials often exhibit distinct optical and electrical properties from their bulk counterparts. In these materials, the spatial confinement of charge carriers and drastically reduced dielectric screening result in enhanced Coulomb interactions[12]. This effect not only leads to large exciton binding energies, but also increased interparticle interactions involving multiple charge carriers. In strongly confined semiconductor quantum dots, the enhanced multi-carrier interaction leads to an ultrafast Auger recombination effect[8], -a nonradiative recombination process that transfers the recombination energy of one electron-hole pair to the remaining charge carriers. Because this process is orders of magnitude faster than radiative recombination processes[13], emission from multi-carrier states such as trions in strongly confined quantum dots is usually faint if detectable at all[14, 15].

Despite the challenges in detecting emission from trions, they are of high technical relevance to quantum information applications. The spin of the extra charge in a trion can essentially be used as a natural two-level quantum system for qubits[3, 16]. Protocols for their applications in quantum repeaters[17], quantum switches[4], and quantum memories[11] have also been proposed. To mitigate the limitations imposed by Auger recombination effects and harvest trions for potential applications, confinement potential engineering has been proposed as an efficient approach to suppress Auger recombination processes and enhance trion emission[18]. In this regard, semiconductor nanoplatelets (NPLs) present an exciting opportunity for hosting trions. Due to their atomic layer thicknesses

and extended lateral sizes, spatial overlap of the electron and hole wavefunctions, and hence the carrier dynamics and interparticle interactions in NPLs are notably different from these of quantum dots[19, 20].

Here, we study the electronic fine structures of NPLs using cryogenic-temperature single particle spectroscopy. The CdSe/CdS/ZnS core/shell/shell NPLs used in this study were synthesized following a previously published method[21]. They consist of four monolayer thick CdSe cores with an average lateral dimension of 21.3 x 6.9 nm^2, and two monolayers of CdS and ZnS shells each conformally wrapping the cores (see Fig. 1a for TEM images of the NPLs). Fig. 1c shows a photoluminescence (PL) spectrum of the ensemble NPLs measured at room temperature with a

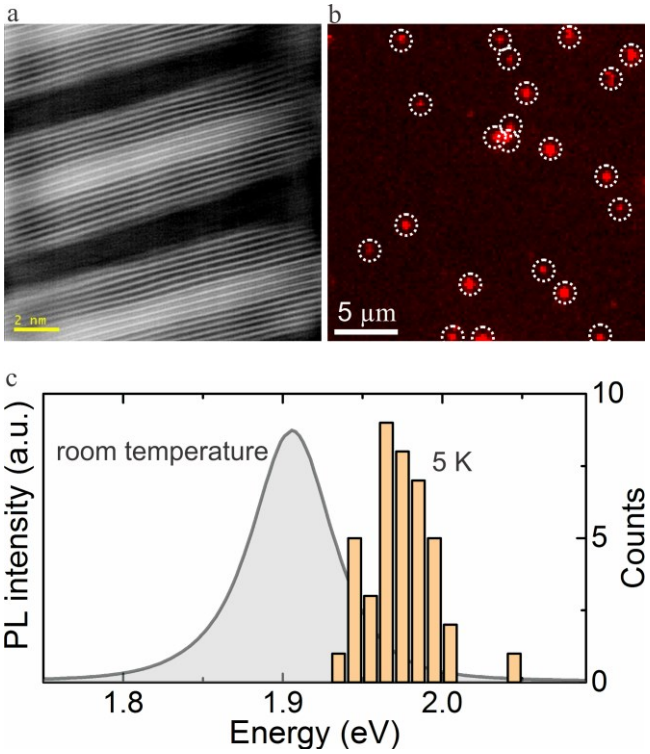

Figure 1. Characterization of the core/shell/shell nanoplatelets. a, A TEM image of the NPLs. **b**, A scanning PL image of scattered NPLs. **c**, PL spectrum of ensemble NPLs measured at room temperature (solid line) and the energy distribution of 41 individual NPLs at 5 K (histogram).

spectral maximum at 1.91 eV. When cooled to 5 K, a blue shift in the PL spectra can be observed. The histogram in Fig. 1c shows PL peak distributions of single NPLs measured at 5 K. This blue shift in PL spectra at low temperature can be attributed to electron-lattice interaction and lattice dilation[22].

The narrow spectral linewidths of the single NPLs at cryogenic temperatures allow us to observe two distinct spectral patterns. In the first type of spectral patterns, the NPLs exhibit single spectral peaks. A representative PL spectral time sequence is shown in Fig. 2a. Single peak emission with a small spectral wandering of less than 0.8 meV can be observed. The line shape of the emission peak clearly follows a Lorentzian function with no detectable phonon sideband (Fig. 2c), likely due to the weak electron-phonon interactions in NPLs[23]. A linewidth of 0.64 meV of the emission peak approaches the lifetime-limited spectral linewidth, consistent with previous reports[19, 24]. In some NPLs, spectral diffusion which manifests itself either as spectral line wandering or inhomogeneous broadening can be observed (see Supplementary Information Section 1). Such signatures have also been observed in zero-dimensional quantum dots[25] and one-dimensional carbon nanotubes[26] and can be ascribed to the quantum confined Stark effect caused by local field fluctuations.

Aside from the single PL peak pattern observed in some NPLs, the other NPLs (30 out of 41) display a different spectral pattern. In these NPLs, two distinct PL peaks with an energy spacing of 5.1 – 16.0 meV can be observed (Fig. 2b and 2d). The average energy spacing ΔE of around 10.5 meV (Fig. 3b) distinguishes this second spectral feature from previously reported phonon sidebands[23] and excimer emission from NPL ensembles[27], which show energy spacings in the range of 20 to 30 meV. Most importantly, the abrupt and correlated switching between the two PL peaks (Fig. 2b) leads us to the conclusion that they are emission from neutral and charged excitons,

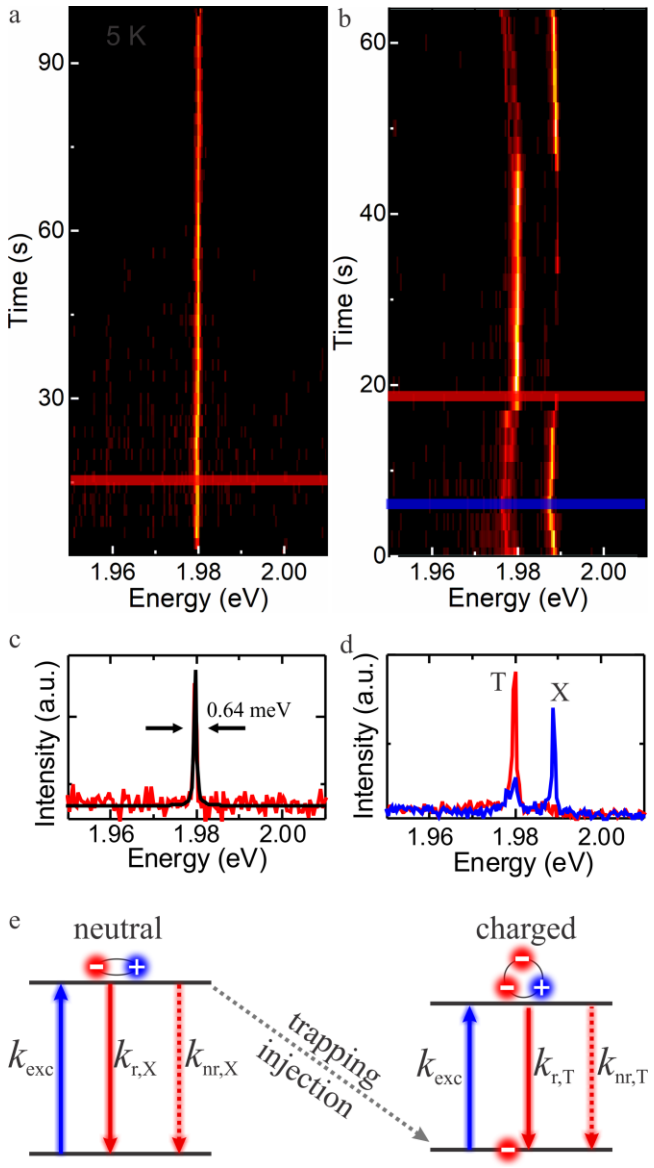

Figure 2. Emission spectra of individual nanoplatelets at 5 K. a, **b**, Time sequences of PL spectra with an integration time of 2 s from two individual NPLs measured at 5 K. A single peak can be observed for the NPL in **a** and two spectral features corresponding to neutral and trion emission can be observed for the NPL in **b**. **c**, **d**, Time integrated PL spectra constructed from the highlighted areas in **a** and **b**. The black curve in **c** is a Lorentzian fit to the spectrum. **e**, Schematic of the energy level diagrams displaying the optical transitions in neutral and charged NPLs. Trapping of a charge carrier leads to the formation of a charged NPL. Excitation of a neutral NPL from the group state generates a neutral exciton, whereas that of a charged NPL leads to a trion.

respectively. When a charge carrier is trapped in a NPL (Fig. 2e), its excitation generates a charged exciton (*i.e*. a trion). Relaxation of the trion back to the charged ground state leads to the emission of a photon – the trion emission. The switch between a neutral and charged NPL can happen on different time scales. In some NPLs, the switch can happen so fast that it is within our integration time, hence the coexistence of the two spectral features in Fig. 2b and 2d. In some other cases, the charged state can persist for many seconds (Supplementary Information Section 2). Variation in the switch time between neutral and charged NPL may be related to the specific local environment that a single NPL is in, and could be effectively controlled by applying gate voltages to the NPLs[28].

To further confirm this assignment, we calculate the band-edge electronic states of the NPLs using an atomistic tight-binding method. We first define the atomistic core-shell-shell geometry of the NPLs. We then calculate the single-particle band edge states using the 20-band $sp^3d^5s^*$ tight-binding model[29, 30]. With the single-particle electron and hole states, we compute the manybody energies of excitons and trions using a configuration interaction approach. Finally, we calculate the emission spectra from the lowest energy complexes utilizing Fermi's Golden Rule (see Methods). A calculated spectrum of a NPL with the same dimensionality as those used in this study is shown in Fig. 3a. Here, the transition energy differences ΔE between the lowest bright neutral (denoted as X) and trion (denoted as T) states are plotted against the normalized oscillator strengths of the states. The trion states, including both the positive (T^+) and negative trions (T^-), appear at the lower energy side of the neutral exciton state, with an energy difference $|\Delta E|$ of 5.5 meV and 11.3 meV, respectively. This confirms our previous assumption that the two spectral features observed in some NPLs originate from neutral excitons and trions, with the low energy peak corresponding to the trions. The average energy spacing of 10.5 meV between the neutral excitons and trions is smaller than that observed in CdSe quantum dots (15 – 22 meV)[31] but larger

than that in quantum wells (0.5 – 1 meV)[32], consistent with the intermediate quantum confinement

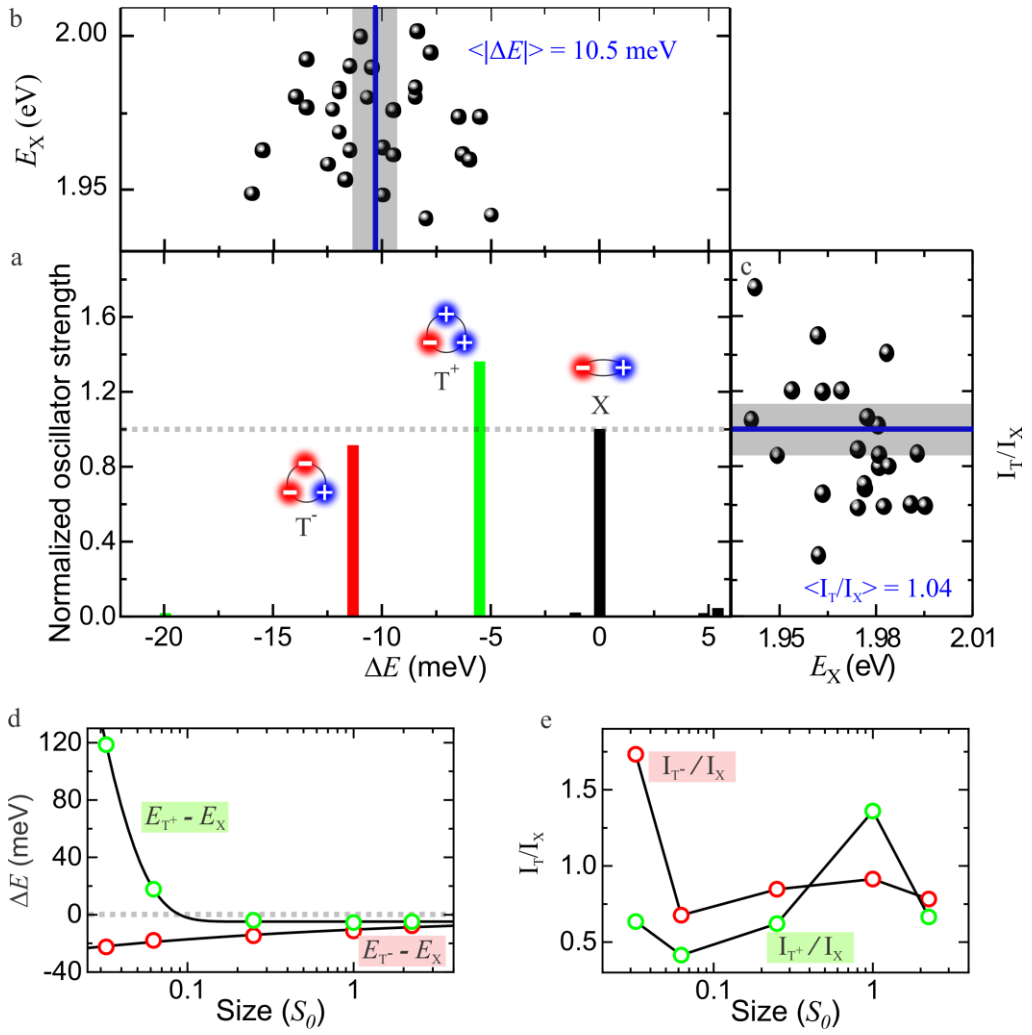

Figure 3. Calculations of band-edge energy states. **a**, Calculated band-edge states including the lowest bright neutral excitons, positive and negative trions. **b**, Energy spacing ΔE between the neutral exciton and trion emission peaks plotted as a function of the neutral exciton energy E_X. The average value $\langle|\Delta E|\rangle$ is 10.5 meV. **c**, Integrated intensity ratio between the neutral exciton and trion emission peaks plotted as a function of the neutral exciton energy. An average value of 1.04 is obtained. **d**, **e**, Lateral size dependent energy spacing ΔE (**d**) and trion/exciton emission intensity ratios (**e**). Here, size of the NPLs are normalized to $S_0 = 21.3 \times 6.9$ nm^2. The solid black lines are guides to the eye.

nature of the NPLs. A comparison between the calculated (Fig.3a) and experimentally measured (Fig. 3b) ΔE further indicates that, while it is unattainable to assign the exact species of trions for each individual NPLs, majority of them likely possess negative trions. This is in an excellent agreement with a recent magneto-optical study of ensemble NPLs[33]. More interestingly, our calculations show that the value of ΔE is highly dependent on the lateral sizes of the NPLs (Fig. 3d). This is especially true in the case of positive trions, which show a crossover from positive values in small NPLs (*i.e.* the positive trion peak appears at the high energy side with respect to the neutral exciton peak) to negative values in large NPLs (*i.e.* the positive trion peak at the low energy side with respect to the neutral exciton peak) (see Supplementary Information Section 3 for calculated spectra of NPLs with various lateral sizes). This size-tunable trion emission may open new opportunities for obtaining bright trion emission at room temperature.

Having confirmed the origin of the two spectral features, we compare their PL intensities. Interestingly, the emission intensity of the trions is slightly higher than that of neutral excitons (Fig. 3c), in reasonable agreement with the theoretically calculated oscillator strength ratios (Fig. 3a). Similar to the ΔE values, a size dependent oscillator strength ratio between the neutral exciton and trion states can be observed (Fig. 3e). This peculiar bright trion emission in NPLs is closely related to their unique carrier dynamics determined by their extended lateral geometries. As discussed earlier, because the nonradiative Auger recombination process in strongly confined low-dimensional materials is typically orders of magnitude faster than the radiative recombination processes, multiexciton emission is severely diminished in these materials. However, the fact that we observe bright trion emission with an intensity comparable to that of neutral excitons indicates that Auger recombination is no longer the dominant recombination channel in charged NPLs. Instead, the radiative decay rate of the charged NPLs has to be comparable to the Auger

recombination rate for the bright trion emission to occur. To verify this, we measure the PL radiative decay rate of the individual NPLs at 5 K and compare it to the previously reported Auger recombination rates of core/shell NPLs[20]. PL intensity-dependent carrier dynamics of the NPLs were measured using a time-tagged time-resolved method. A representative PL time trace of an individual NPL at 5 K is shown in Fig. 4a (see Supplementary Information S4 for photo-correlation measurements verifying the single particle nature of the measured NPLs), where no drastic PL fluctuation or blinking is observed. Using a previously established method in which the maximum PL intensity periods in a time trace were considered to have a unity quantum yield and the corresponding lifetime solely contributed by the radiative recombination process[34, 35], we derive

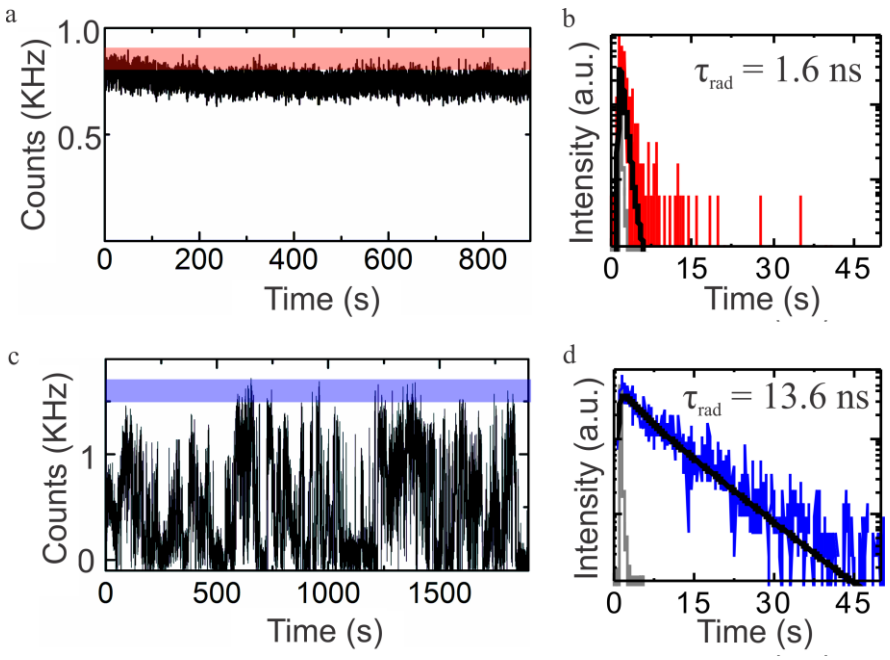

Figure 4. Carrier dynamics of the nanoplatelets. a, **c**, PL time traces of individual NPLs measured at 5 K (**a**) and room temperature (**c**). **b**, **d**, PL decay curves constructed from the maximum PL intensity periods highlighted in **a** and **c**. Gray curves: the instrument response function. Black curves: single exponential fittings to the decay curves by deconvoluting the instrument response function.

the radiative decay rates of the NPLs by constructing PL decay curves from the maximum PL intensity periods. Fig. 4b shows one such example and it can be well fit with a single exponential function by deconvoluting the instrument response function. This yields a corresponding radiative lifetime of 1.60 ns. Performing similar measurements on 33 individual NPLs at 5 K gives an average radiative lifetime of 1.28 ns (see Supplementary Information S5 for histograms). We note that the radiative lifetime measured here might be that of the neutral excitons, trions, or both species because from the PL time traces we cannot distinguish the emission from neutral or charged excitons. However, this value sets an upper limit for the radiative lifetime of the trions, which typically decays a few times faster than neutral excitons (*i.e.* $k_{r,T} > k_{r,X}$ in Fig. 2e)[36].

This average radiative lifetime of 1.28 ns at 5 K is nearly one order of magnitude smaller than that measured at room temperature using a similar method, which is found to be around 13.7 ns (Fig. 4d and Supporting Information S4 for distribution). The reduction in the radiative lifetime with temperature also explains the suppressed PL blinking/fluctuation at 5 K (Fig. 4a, 4c) for the reason that the radiative decay process becomes more predominant compared to nonradiative channels. This fast radiative decay rate (1/1.28 ns) makes it comparable to Auger recombination rates in core/shell NPLs of similar compositions and sizes, which were measured to be around 1/2 ns[20], remarkably smaller than those in quantum dots[13]. With that, we infer that the bright trion emission in core/shell NPLs at 5 K can be attributed to two major reasons – the fast radiative decay rate at low temperatures and the inhibited Auger recombination processes, both due to the extended lateral geometries of the NPLs.

These findings indicate that NPLs, with their unique lateral size-dependent carrier dynamics, present an interesting material platform for harvesting multi-carrier emission. By applying gate voltages, extra charge carriers can be deterministically injected one-by-one into the NPLs to

generate bright trion emission. Energy spacing between the trion and exciton states can be tuned by the NPL lateral sizes so that room temperature trion emission is attainable. These distinct trion features in NPLs pose an exciting opportunity for their applications in lasing[37], light-emitting diodes[38], and quantum logic devices[4, 6, 11, 17].

Methods

Optical Measurements of Single Nanoplatelets. Samples for single particle optical measurements were prepared by spin coating diluted solutions of nanoplatelets onto quartz substrates. For cryogenic temperature measurements, the substrates were immersed in liquid helium in a bath cryostat that is coupled to a home-built confocal laser microscope. A pulsed diode laser with a wavelength of 400 nm was focused onto the samples by a microscope objective (60X, NA = 1.40 or 60X, NA = 0.7). Emission from the samples was collected by the same objective and sent to a CCD camera installed on a 500 mm spectrograph for imaging and spectroscopy measurements. Time-resolved photoluminescence and photon correlation measurements were performed using two single photon avalanche diodes in a Hanbury-Brown and Twiss geometry. A time-correlated single photon counting electronic system from PicoQuant (HydraHarp 400) was used for these measurements.

Atomistic tight-binding calculations. Electronic and optical properties of the NPLs were computed using the QNANO code[29, 30]. To define the atomistic geometry of the NPLs, four monolayer cores of zincblende CdSe with lattice constant 6.02 Angstroms with various lateral dimensions were generated. A two monolayer conformal shell of zincblende CdS, followed by a two monolayer conformal shell of zincblende ZnS were then added. Due to the lattice mismatch

of the core and shells, we then relaxed the atomic positions using a Keating valence force field model, resulting in the final atomic positions.

To calculate the single-particle band edge state, a 20 band $sp^3d^5s^*$ model was used as the basis on each atom. The tight-binding parameters were fit to density functional theory calculations of the band structures of bulk materials of zincblende CdSe, CdS, and ZnS separately. To ensure that the fit parameters were consistent, initial guesses based on analytic solutions to the $sp^3d^5s^*$ model were used. The manybody energies and wavefunctions of the excitons and trions were calculated using full configuration interaction of the manybody Hamiltonian. The number of band-edge hole and electron states included in the manybody was chosen such that the resulting energies were converged to less than a meV (see Supporting Information S6).

Supplementary information

The following files are available free of charge. Spectral diffusion in single nanoplatelets; trion emission in single nanoplatelets; calculation of band-edge states in NPLs with various lateral sizes; second-order photon-correlation measurements of single nanoplatelets; radiative lifetime distributions of the nanoplatelets; convergence of excitonic complex energies (PDF).

Acknowledgements

This work was performed, in part, at the Center for Nanoscale Materials, a U.S. Department of Energy, Office of Science, Office of Basic Energy Sciences User Facility under contract no. DE-AC02-06CH11357. I. C., A. H. and D. V. T acknowledge support by NSF under award number CHE-1611331 and by the Department of Defense (DOD) Air Force Office of Scientific Research under grant number FA9550-18-1-0099.

Corresponding Author

E-mail: xuedan.ma@anl.gov

Competing final interests

The authors declare no competing financial interest.

References

1. Wojs, A.; Hawrylak, P. Negatively charged magnetoexcitons in quantum dots. *Phys Rev B*, **51**, 10880-10885 (1995).

2. De Greve, K.; Yu, L.; McMahon, P. L.; Pelc, J. S.; Natarajan, C. M.; Kim, N. Y.; Abe, E.; Maier, S.; Schneider, C.; Kamp, M.; Höfling, S.; Hadfield, R. H.; Forchel, A.; Fejer, M. M.; Yamamoto, Y. Quantum-dot spin–photon entanglement via frequency downconversion to telecom wavelength. *Nature*, **491**, 421-425 (2012).

3. Gao, W. B.; Fallahi, P.; Togan, E.; Miguel-Sanchez, J.; Imamoglu, A. Observation of entanglement between a quantum dot spin and a single photon. *Nature*, **491**, 426-430 (2012).

4. Sun, S.; Kim, H.; Solomon, G. S.; Waks, E. A quantum phase switch between a single solid-state spin and a photon. *Nat Nanotechnol*, **11**, 539-545 (2016).

5. Delteil, A.; Sun, Z.; Gao, W.-B.; Togan, E.; Faelt, S.; Imamoğlu, A. Generation of heralded entanglement between distant hole spins. *Nat Phys*, **12**, 218-223 (2016).

6. Gao, W. B.; Fallahi, P.; Togan, E.; Delteil., A.; Chin, Y. S.; Miguel-Sanchez, J.; Imamoglu, A. Quantum teleportation from a propagating photon to a solid-state spin qubit. *Nat Commun*, **4**, 2744 (2013).

7. Kagan, C. R.; Lifshitz, E.; Sargent, E. H.; Talapin, D. V. Building devices from colloidal quantum dots. *Science*, **353**, aac5523 (2016).

8. Klimov, V. I.; Mikhailovsky, A. A.; McBranch, D. W.; Leatherdale, C. A.; Bawendi, M. G. Quantization of Multiparticle Auger Rates in Semiconductor Quantum Dots. *Science*, **287**, 1011-1013 (2000).

9. Ithurria, S.; Tessier, M. D.; Mahler, B.; Lobo, R. P. S. M.; Dubertret, B.; Efros, Al. L. Colloidal nanoplatelets with two-dimensional electronic structure. *Nat Mater*, **10**, 936-941 (2011).

10. Grim, J. Q.; Christodoulou, S.; Stasio, F. D.; Krahne, R.; Cingolani, R.; Manna, L.; Moreels, I. Continuous-wave biexciton lasing at room temperature using solution-processed quantum wells. *Nat Nanotechnol*, **9**, 891-895 (2014).

11. Kroutvar, M.; Ducommun, Y.; Heiss, D.; Bichler, M.; Schuh, D.; Abstreiter, G.; Finley, J. J. Optically programmable electron spin memory using semiconductor quantum dots. *Nature*, **432**, 81-84 (2004).

12. Franceschetti, A.; Fu, H.; Wang, L. W.; Zunger, A. Many-body pseudopotential theory of excitons in InP and CdSe quantum dots. *Phys Rev B*, **60**, 1819-1829 (1999).

13. Wang, L.-W.; Califano, M.; Zunger, A.; Franceschetti, A. Pseudopotential Theory of Auger Processes in CdSe Quantum Dots. *Phys Rev Lett*, **91**, 056404 (2003).

14. Gómez, D. E.; van Embden, J.; Mulvaney, P.; Fernée, M. J.; Rubinsztein-Dunlop, H. Exciton−Trion Transitions in Single CdSe–CdS Core–Shell Nanocrystals. *ACS Nano*, **3**, 2281-2287 (2009).

15. Spinicelli, P.; Buil, S.; Quelin, X.; Mahler, B.; Dubertret, B.; Hermier, J.-P. Bright and Grey States in CdSe-CdS Nanocrystals Exhibiting Strongly Reduced Blinking. *Phys Rev Lett*, **102**, 136801 (2009).

16. Press, D.; Ladd, T. D.; Zhang, B.; Yamamoto, Y. Complete quantum control of a single quantum dot spin using ultrafast optical pulses. *Nature*, **456**, 218-221 (2008).

17. Wang, T.-J.; Song, S.-Y.; Long, G. L. Quantum repeater based on spatial entanglement of photons and quantum-dot spins in optical microcavities. *Phys Rev A*, **85**, 062311 (2012).

18. Cragg, G. E.; Efros, A. L. Suppression of Auger Processes in Confined Structures. *Nano Lett*, **10**, 313-317 (2010).

19. Naeem, A.; Masia, F.; Christodoulou, S.; Moreels, I.; Borri, P.; Langbein, W. Giant exciton oscillator strength and radiatively limited dephasing in two-dimensional platelets. *Phys Rev B*, **91**, 121302(R) (2015).

20. Pelton, M.; Andrews, J. J.; Fedin, I.; Talapin, D. V.; Leng, H.; O'Leary, S. K. Nonmonotonic Dependence of Auger Recombination Rate on Shell Thickness for CdSe/CdS Core/Shell Nanoplatelets. *Nano Lett*, **17**, 6900–6906 (2017).

21. Ithurria, S.; Talapin, D. V. Colloidal Atomic Layer Deposition (c-ALD) using Self-Limiting Reactions at Nanocrystal Surface Coupled to Phase Transfer between Polar and Nonpolar Media. *J Am Chem Soc*, **134**, 18585–18590 (2012).

22. Varshni, Y. P. Temperature dependence of the energy gap in semiconductors. *Physica*, **34**, 149-154 (1967).

23. Achtstein, A. W.; Schliwa, A.; Prudnikau, A.; Hardzei, M.; Artemyev, M. V.; Thomsen, C.; Woggon, U. Electronic Structure and Exciton−Phonon Interaction in Two-Dimensional Colloidal CdSe Nanosheets. *Nano Lett*, **12**, 3151−3157 (2012).

24. Tessier, M. D.; Javaux, C.; Maksimovic, I.; Loriette, V.; Dubertret, B. Spectroscopy of Single CdSe Nanoplatelets. *ACS Nano*, **6**, 6751–6758 (2012).

25. Empedocles, S. A.; Bawendi, M. G. Quantum-Confined Stark Effect in Single CdSe Nanocrystallite Quantum Dots. *Science*, **278**, 2114-2117 (1997).

26. Ma, X.; Roslyak, O.; Wang, F.; Duque, J. G.; Piryatinski, A.; Doorn, S. K.; Htoon, H. Influence of Exciton Dimensionality on Spectral Diffusion of Single-Walled Carbon Nanotubes. *ACS Nano*, **8**, 10613-10620 (2014).

27. Diroll, B. T.; Cho, W.; Coropceanu, I.; Harvey, S. M.; Brumberg, A.; Holtgrewe, N.; Crooker, S. A.; Wasielewski, M. R.; Prakapenka, V. B.; Talapin, D. V.; Schaller, R. D. Semiconductor nanoplatelet excimers. *Nano Lett*, **18**, 6948-6953 (2018).

28. Warburton, R. J.; Schäflein, C.; Haft, D.; Bickel, F.; Lorke, A.; Karrai, K.; Garcia, J. M.; Schoenfeld, W.; Petroff, P. M. . Optical emission from a charge-tunable quantum ring. *Nature*, **405**, 926-929 (2000).

29. Zieliński, M.; Korkusiński, M.; Hawrylak, P. Atomistic tight-binding theory of multiexciton complexes in a self-assembled InAs quantum dot. *Phys Rev B*, **81**, 085301 (2010).

30. Hartmann, N. F.; Otten, M.; Fedin, I.; Talapin, D.; Cygorek, M.; Hawrylak, P.; Korkusinski, M.; Gray, S.; Hartschuh, A.; Ma, X. Uniaxial Transition Dipole Moments in Semiconductor Quantum Rings Caused by Broken Rotational Symmetry. *Nat Commun*, DOI: 10.1038/s41467-41019-11225-41466 (2019).

31. Shimizu, K. T.; Woo, W. K.; Fisher, B. R.; Eisler, H. J.; Bawendi, M. G. Surface-Enhanced Emission from Single Semiconductor Nanocrystals. *Phys Rev Lett*, **89**, 117401 (2002).

32. Solovyev, V. V.; Kukushki, I. V. Measurement of binding energy of negatively charged excitons in GaAs/$Al_{0.3}Ga_{0.7}$As quantum wells. *Phys Rev B*, **79**, 233306 (2009).

33. Shornikova, E. V.; Biadala, L.; Yakovlev, D. R.; Feng, D.; Sapega, V. F.; Flipo, N.; Golovatenko, A. A.; Semina, M. A.; Rodina, A. V.; Mitioglu, A. A.; Ballottin, M. V.; M. Christianen, P. C.; Kusrayev, Y. G.; Nasilowski, M.; Dubertret,B.; Bayer, M. Electron and Hole g-Factors and Spin Dynamics of Negatively Charged Excitons in CdSe/CdS Colloidal Nanoplatelets with Thick Shells. *Nano Lett*, **18**, 373-380 (2018).

34. Fisher, B. R.; Eisler, H.-J.; Stott, N. E.; Bawendi, M. G. Emission Intensity Dependence and Single-Exponential Behavior In Single Colloidal Quantum Dot Fluorescence Lifetimes. *J Phys Chem B*, **108**, 143-148 (2004).

35. Ma, X.; Diroll, B. T.; Cho, W.; Fedin, I.; Schaller, R. D.; Talapin, D. V.; Gray, S. K.; Wiederrecht, G. P.; Gosztola, D. J. Size-Dependent Biexciton Quantum Yields and Carrier Dynamics of Quasi-Two-Dimensional Core/Shell Nanoplatelets. *ACS Nano*, **11**, 9119-9127 (2017).

36. Park, Y.-S.; Bae, W. K.; Pietryga, J. M.; Klimov, V. I. Auger Recombination of Biexcitons and Negative and Positive Trions in Individual Quantum Dots. *ACS Nano*, **8**, 7288-7296 (2014).

37. Wu, K.; Park, Y.-S.; Lim, J.; Klimov, V. I. Towards zero-threshold optical gain using charged semiconductor quantum dots. *Nat Nanotechnol*, **12**, 1140-1147 (2017).

38. Ross, J. S.; Klement, P.; Jones, A. M.; Ghimire, N. J.; Yan, J.; Mandrus, D. G.; Taniguchi, T.; Watanabe, K.; Kitamura, K.; Yao, W.; Cobden, D. H.; Xu, X. Electrically tunable excitonic light-emitting diodes based on monolayer WSe2 p–n junctions. *Nat Nanotechnol*, **9**, 268-272 (2014).